EPR investigation of Pt^- in silicon

Frederick G. Anderson, Robert F. Milligan,* and George D. Watkins
Department of Physics and Sherman Fairchild Center, Lehigh University, Bethlehem, Pennsylvania 18015
(Received 10 June 1991)

Using EPR we have resolved the question of whether the dominant Pt^- defect in silicon consists of an isolated platinum ion or a platinum-platinum pair. We have measured the uniaxial-stress-induced shifts in the g values and find that the stress-coupling tensor shows the defect symmetry to be C_{2v}. By selective doping with ^{195}Pt and ^{198}Pt, we demonstrate that there is no hyperfine evidence of a second platinum. We therefore conclude that the original model of Woodbury and Ludwig of an isolated substitutional platinum impurity that spontaneously distorts off center in a $\langle 100 \rangle$ direction is correct. We have also measured the defect realignment under stress, which occurs even at pumped-liquid-helium temperatures. We find that the sense of the alignment for this platinum defect is opposite to that for the negative vacancy. In addition, we have fully resolved the superhyperfine interaction involving the two nearest-neighbor silicon atoms. Lastly, we observe a shift in the g values depending upon the nuclear isotopes of these two nearest-neighbor silicon atoms.

I. INTRODUCTION

Electron paramagnetic resonance (EPR) of platinum in silicon was first observed by Woodbury and Ludwig.[1,2] Based on the anisotropy of the g tensor and the hyperfine tensor, they proposed that the spectrum resulted from a single isolated substitutional Pt^- ion that had distorted spontaneously off center in a $\langle 100 \rangle$ direction, resulting in a defect of orthorhombic (C_{2v}) symmetry. More than 20 years later, Henning and Egelmeers reported results of strain-modulated EPR experiments of the spectrum,[3] and proposed instead that it resulted from a Pt-Pt pair in which a second interstitial Pt^0 atom lies near the substitutional Pt^- ion. As evidence, they cited partially resolved structure on each line of the spectrum that could result from hyperfine interaction with the second Pt^0 atom. Further, from the analysis of the strain-induced changes in the g tensor, they deduced a lower symmetry (C_{1h}) for the defect.

The present study was initiated to resolve this question and to investigate further the Pt^- defect in silicon. In this first paper (I), we present our experimental results using EPR to probe further the structure of the defect. These experiments involved selective isotope doping with ^{195}Pt and ^{198}Pt to test the possible presence of a second Pt^0 atom, and the application of uniaxial stress to measure directly the changes induced in the g tensor and the defect realignment induced by the stress. In addition, we have fully resolved the hyperfine interaction with the nearest-neighbor silicon atoms. Our results fully support the original conclusion of Woodbury and Ludwig that the defect is composed of an *isolated* substitutional platinum impurity that has undergone a $\langle 100 \rangle$ off-center distortion.

In the course of this study, we have observed a remarkable new effect: A shift of the g values for the Pt^- center depending upon the nuclear isotopes of the nearest-neighbor silicon atoms. To our knowledge, this is the first observation of an isotope effect on the g values for a defect in any semiconductor.[4] It is particularly remarkable in that it is an isotope effect for the *neighbors* of the platinum.

In a companion paper (II) immediately following this one,[5] we develop in detail the "vacancy model" that one of us (G.D.W.) has proposed for substitutional transition-metal defects at the heavy end of each transition-metal series.[6] Using the results presented in this paper, we test the validity of the model through its applicability to the Pt^- defect in silicon. We conclude that the vacancy model satisfactorily explains the EPR spectrum of the Pt^- defect and does so more completely than various alternative models that have been suggested.

The organization of the present paper (I) is as follows. In Sec. II, we describe the details of our experiments. The results are presented in Sec. III. Finally, the results are discussed and interpreted in Sec. IV.

II. EXPERIMENTAL DETAILS

Two electron-paramagnetic-resonance spectrometers, one operating at 14 GHz, the other at 20 GHz, were used during the course of these experiments. The 20-GHz spectrometer was used for most of the experiments concerning unstressed samples. Experiments involving static uniaxial stress were performed using the 14-GHz spectrometer. In either case, experiments were performed in the absorption mode at liquid-helium temperatures (4 or 2 K).

In order to determine all of the coefficients coupling stress to shifts in the g value, stress perpendicular and parallel to the magnetic field was required. Perpendicular stress was applied via a rod that was inserted vertically into the TE_{011} cylindrical cavity. The rod was supported from below by the vertically mounted sample in the center of the cylindrical TE_{011} cavity. The rod itself supported a lever, outside of the cryostat, on which several

weights were hung.

For stress parallel to the magnetic field, a rectangular cavity was employed with the sample being placed horizontally on the short side of the cavity. Stress was applied via a plunger inserted horizontally through the wall of the cavity. A lever, located inside the cryostat, pushed against this plunger. Calibrating the amount of stress was achieved by rotating the magnetic field so that the field was perpendicular to the direction of the applied stress, and using the previous results obtained from the perpendicular geometry.

To study defect alignment under stress, only the perpendicular geometry was required. Line intensities were obtained by digitizing the recorded spectra and integrating twice numerically using an IBM CS-9000 computer.

The samples were prepared from floating-zone silicon with approximately $2-5\times10^{16}$ cm^{-3} shallow-donor concentration (P or As). Fine platinum powder (either ^{195}Pt or ^{198}Pt isotope enriched, or Pt in natural concentration) was rubbed into the pits of a freshly etched (hot KOH) surface of the silicon. The samples were then heated to 1200 °C for 15–20 h under a small flow of He gas, and subsequentially quenched to room temperature in ethylene glycol.[7] After the quench, the sample surfaces were ground to the desired dimensions and etched to make their dimensions square and to remove the silicate layer that had formed on the surface during the diffusion process. The platinum defect is found to be stable at room temperature.

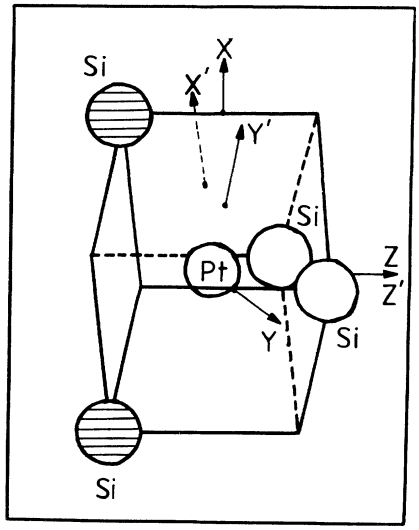

FIG. 1. Model for the Pt^- defect in Si. Shown in this figure is that oriented defect for which the shaded Si atoms give rise to the superhyperfine interaction. Shown are the principal axes of the defect (x,y,z), and a set of defect cubic axes (x',y',z').

III. EXPERIMENTAL RESULTS

A. EPR spectrum

The spin Hamiltonian (effective spin $\mathcal{S}=\frac{1}{2}$) that describes the platinum spectrum is

$$\mathcal{H}=\mu_B\mathbf{B}\cdot\underline{g}\cdot\mathcal{S}+\mathcal{S}\cdot\underline{A}\cdot\mathbf{I}+\sum_k \mathcal{S}\cdot\underline{T}_k\cdot\mathbf{I}_k\ , \tag{1}$$

where μ_B is the Bohr magneton, $\mathbf{B}$ is the applied magnetic field, and $\mathcal{S}$, $\mathbf{I}$, and $\mathbf{I}_k$ are the spins of the electron, the platinum nucleus, and the nuclei of two of the four nearest-neighbor silicon atoms, respectively. In the principal axis system of the defect, the $\underline{g}$ and $\underline{A}$ tensors are diagonal. This axis system is shown in Fig. 1. The ⟨100⟩ axis along which the platinum spontaneously distorts is labeled the z axis. We then label the x axis, which is in a ⟨110⟩ direction, such that the two nearest-neighbor silicon atoms giving rise to the resolved hyperfine interaction lie in the xz plane. The y axis is in the remaining mutually perpendicular ⟨110⟩ direction. Shown in addition are a set of cubic defect axes (x',y',z'), coinciding with the crystalline ⟨100⟩ axes, which will be used later.

The first term in Eq. (1) describes the Zeeman interaction between the paramagnetic electron and the magnetic field. The principal g values are given in Table I. A plot of g versus direction of magnetic field, as the field is rotated about several of the crystalline axes, is given in Fig. 2.

The second term in Eq. (1) describes the hyperfine interaction with the ^{195}Pt nucleus, which has $I=\frac{1}{2}$ and a natural abundance of 33.8%. The effect of this term is to produce two satellite lines, arising from those defects with a ^{195}Pt ion, centered around each single line in the spectrum, arising from those defects with a ^{198}Pt ($I=0$) ion that comprises the remaining 66.2% of natural platinum. Figure 3 shows this structure for two samples, one enriched with ^{195}Pt, and the other enriched with ^{198}Pt. The principal A values are also given in Table I.

The final term in the spin Hamiltonian represents the hyperfine interaction with the nearest-neighbor silicon atoms. (^{29}Si is 4.7% abundant and has $I=\frac{1}{2}$.) An interaction with two equivalent silicon sites is observed, producing additional satellites on each spectral component, as indicated in Fig. 4. The components of $\underline{T}_k$ are given in Table I using the defect principal axis system.

TABLE I. The principal values of the $\underline{g}$ and $\underline{A}$ tensors for Pt^- in silicon. The $\underline{T}$ tensor giving the superhyperfine interaction with the two nearest-neighbor silicon atoms is not diagonal in the principal-axis system.

Principal direction	g	A (10^{-4} cm^{-1})	T_k (10^{-4} cm^{-1})		
x	1.3865	148	36.55	0	±1.76
y	1.4265	186	0	24.87	0
z	2.0789	127	±1.76	0	27.31

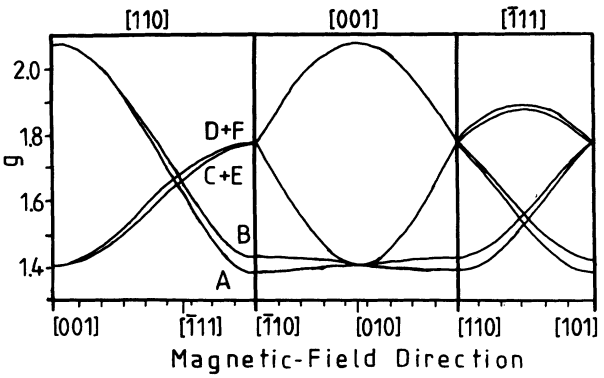

FIG. 2. Plot of g for variously oriented Pt^- defects as a function of magnetic-field direction, given at the bottom of the plot, as the magnetic field is rotated about the crystalline axes labeled at the top of each plot. The labeling of the curves A and B in the left-hand panel agrees with Woodbury and Luwdig (Ref. 1), and C–F agrees with the labeling of Henning and Egelmeers (Ref. 3).

The plus and minus signs of the off-diagonal elements refer to the two different sites. Diagonalizing $\underline{T}_k$ gives principal values of 36.9×10^{-4}, 24.9×10^{-4}, and 27.0×10^{-4} cm^{-1}. In its diagonalized form, $\underline{T}_k$ has approximately axial symmetry, with the symmetry axis lying in the xz plane and being tilted $\pm10.4°$ from the x axis.

The origin of the partially resolved shoulders on each of the three main lines in Fig. 3 has been the subject of some discussion. Henning and Egelmeers concluded that they resulted from hyperfine interaction involving a second Pt atom. The relative intensities 1:4:1 matched well with the value of $1:2(1-a)/a:1$ predicted with $a=0.34$, the natural abundance of ^{195}Pt in their unenriched samples. It is clear from Fig. 3, however, that this structure is independent of the ^{195}Pt and ^{198}Pt concentrations, and therefore cannot be due to a ^{195}Pt hyperfine interaction involving a second platinum atom.[8] Instead, we conclude, as did Woodbury and Ludwig,[1] that these shoulders arise from hyperfine interaction involving additional neighboring silicon atoms. In the companion paper (II), it is suggested that these shoulders result in part from hyperfine interaction with the nearest-neighbor pair of silicon atoms in the yz plane, i.e., the unshaded silicon atoms in Fig. 1.

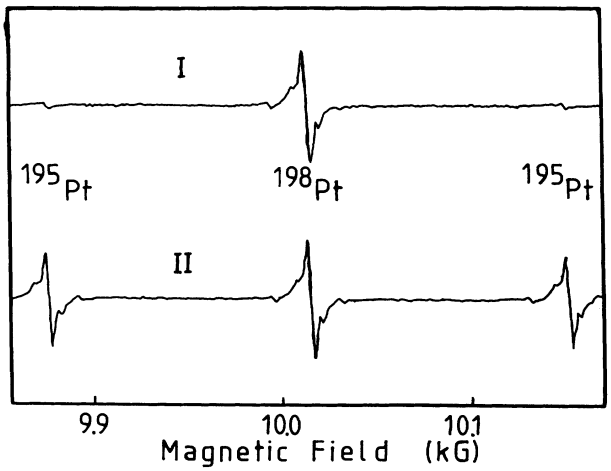

FIG. 3. EPR spectra at 4.2 K, $\mathbf{B}\|\langle110\rangle$, and $\nu_{micro}=20$ GHz of the line A in Fig. 2 for samples of two different isotopic enrichments; (I) 10% ^{195}Pt, 90% ^{198}Pt, and (II) 60% ^{195}Pt, 40% ^{198}Pt.

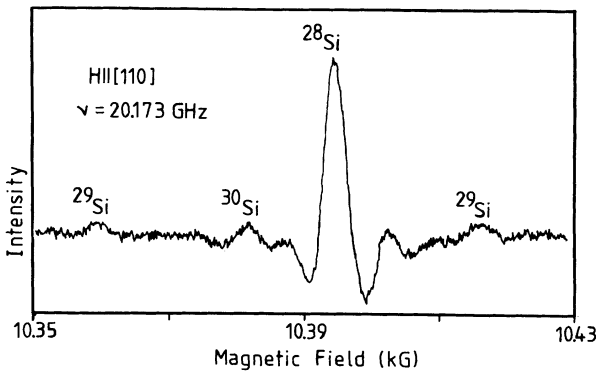

FIG. 4. EPR spectra at 4.2 K, $\mathbf{B}\|\langle110\rangle$, and $\nu_{micro}=20$ GHz of the line A in Fig. 2. The lock-in amplifier is tuned to the second harmonic of the magnetic-field modulation resulting in a line shape appearing like the second derivative of absorption.

Our experiments analyzing the hyperfine lines have led to a very interesting observation, an isotope effect on the g values. Figure 4 shows the resonance with the magnetic field pointing along the x axis. In this case, to improve resolution, our lock-in amplifier was tuned to the second harmonic of the magnetic field modulation, resulting in a line shape of the form of the second derivative of absorption. The idea of an isotope effect was first recognized when we noticed that the average of the two hyperfine peaks due to the presence of a ^{29}Si atom as a nearest neighbor did not coincide with the main peak, as is clearly evident in Fig. 4. (Second-order effects are negligible.) If this is an isotope effect, we would expect a single line due to the presence of a ^{30}Si atom at twice the shift in field. (^{30}Si is 3% abundant with spin $I=0$.) This is

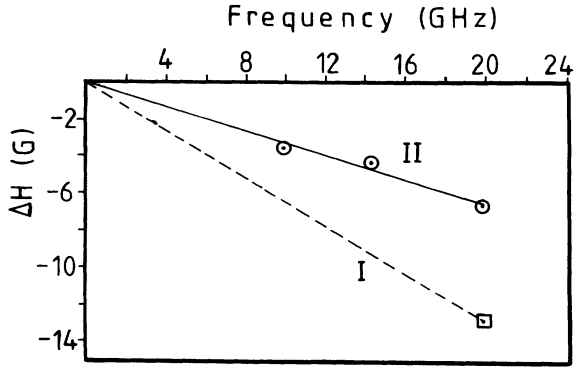

FIG. 5. Plot showing the shift in magnetic field relative to the central line vs microwave frequency of (I) the ^{30}Si-^{28}Si satellite, and (II) the average of the two ^{29}Si-^{28}Si satellites. The magnetic field is along the x axis (line A in Fig. 2).

TABLE II. The Si-neighbor isotope shifts in the principal g values using the ^{28}Si-^{28}Si line as reference.

	^{29}Si	^{30}Si
Δg_1	0.0012	0.0021
Δg_2	0.0006	0.0013
Δg_3	0.0009	0.0020

indeed observed, as shown in Fig. 4.

If this is a shift in the g value, the shift in magnetic-field position should increase linearly with microwave frequency. In Fig. 5, we combine the results from our 14- and 20-GHz measurements with our estimates from Fig. 2 of Ref. 3 at 10 GHz. The linear dependence is clearly demonstrated, as well as the proportionality to the change in mass Δm.

We conclude, therefore, that the g values for the defect are different depending upon whether the nearest-neighbor silicon pair is ^{28}Si-^{28}Si, ^{29}Si-^{28}Si, or ^{30}Si-^{28}Si. The relative intensities of the central ^{28}Si-^{28}Si component, the ^{29}Si-^{28}Si hyperfine satellites, and the shifted ^{30}Si-^{28}Si satellite confirm the two silicon dependence. With the central ^{28}Si-^{28}Si line as a reference, the shifts in the g values are given in Table II.

The inequivalence of the two silicon neighbors resulting from the different isotopes actually lowers the symmetry of the center from C_{2v} to C_{1h}. As a result, the isotope shifted g need not have the same principal axes as the dominant ^{28}Si-^{28}Si center. However, no evidence of splitting of the ^{30}Si-^{28}Si line is observed in angular dependence studies measured in the xz plane.

B. Uniaxial stress

The effects of uniaxial stress on the spectrum are illustrated in Figs. 6, 7, and 8. Two effects are observed (see Fig. 6.): The resonance lines shift in field position, and at the same time some resonances increase in intensity while others decrease. We consider first the shifts in the field positions.

1. $\underline{g}$ tensor

The shifts in the spectral line positions can be described by an additional term in the spin Hamiltonian of the form

$$\mathcal{H}_z^s = \mu_B \mathbf{B} \cdot \delta\underline{g} \cdot \mathcal{S} , \tag{2}$$

where

$$\delta g_{kl} = \sum_{i,j} G_{ijkl} \sigma_{ij} \quad (\delta\underline{g} = \underline{G} \cdot \underline{\sigma}) . \tag{3}$$

Here, the fourth-order stress coupling tensor $\underline{G}$ provides the proportionality between the applied stress tensor $\underline{\sigma}$ and the tensor giving the shift in the g values $\delta\underline{g}$. Because both $\delta\underline{g}$ and $\underline{\sigma}$ are symmetric tensors, each can be rewritten more compactly in the six-component Voigt matrix notation. In the defect principal axis system, and taking account of the C_{2v} symmetry of the defect, this becomes

$$\begin{bmatrix} \delta g_{xx} \\ \delta g_{yy} \\ \delta g_{zz} \\ \delta g_{yz} \\ \delta g_{zx} \\ \delta g_{xy} \end{bmatrix} = \begin{bmatrix} G_1 & G_4 & G_7 & 0 & 0 & 0 \\ G_2 & G_5 & G_8 & 0 & 0 & 0 \\ G_3 & G_6 & G_9 & 0 & 0 & 0 \\ 0 & 0 & 0 & G_{10} & 0 & 0 \\ 0 & 0 & 0 & 0 & G_{11} & 0 \\ 0 & 0 & 0 & 0 & 0 & G_{12} \end{bmatrix} \begin{bmatrix} \sigma_{xx} \\ \sigma_{yy} \\ \sigma_{zz} \\ \sigma_{yz} \\ \sigma_{zx} \\ \sigma_{xy} \end{bmatrix} . \tag{4}$$

For a center of C_{2v} symmetry, there are 12 independent, nonzero elements of the matrix $\underline{G}$. A lower-symmetry center has additional elements.

The elements of $\underline{G}$ were determined by applying stress in the crystalline ⟨100⟩, ⟨110⟩, and ⟨111⟩ directions and measuring the shifts in the resonance line positions for the differently oriented defects at several magnetic-field orientations. The experimental results are summarized in Fig. 7 and tabulated in Table III. The off-diagonal elements in the upper block of $\underline{G}$ were determined with stress that was perpendicular to the magnetic field. The upper three diagonal matrix elements describe shifts of the g values parallel to the applied stress, deter-

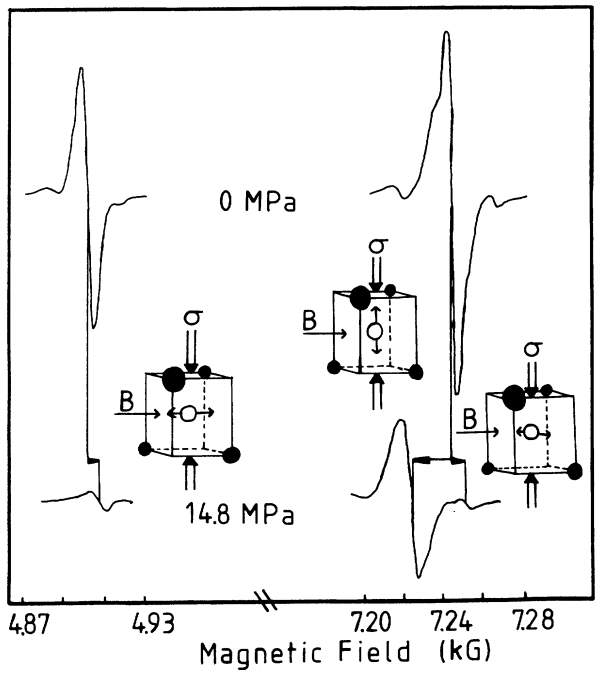

FIG. 6. EPR spectra at 4.2 K showing the effects of ⟨100⟩ uniaxial stress on the spectrum: (I) a shift in the g values, and (II) defect realignment. The upper spectra were recorded in the absence of stress. The left-hand resonance is from defects with Pt distortion parallel to the magnetic field, the right-hand from defects with Pt distortion perpendicular (see insets). Under ⟨100⟩ stress perpendicular to the magnetic field (lower spectra), the left-hand resonance shifts in magnetic field and the right-hand splits into two, corresponding to Pt distortions parallel and perpendicular to the stress. The intensity of the resonance for defects with Pt distortion parallel to the stress is stronger than that for defects with Pt distortion perpendicular.

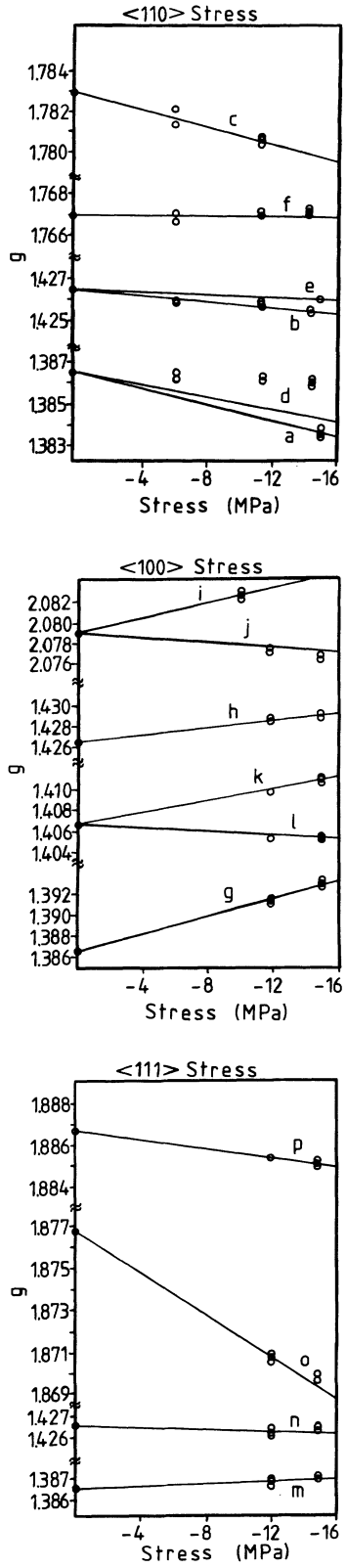

FIG. 7. Shifts in the g values vs stress. The labels define the magnetic field and defect orientation for each spectral component as given in Table III. The crystalline directions of the uniaxial stress are indicated at the tops of the plots. The solid lines are the calculated shifts using the components of $\underline{G}$ given in Table III.

TABLE III. The directions of the applied uniaxial stress and the magnetic field, expressed in the defect principal-axis system (x,y,z), for the various plots in Fig. 7. The solid lines in Fig. 7 represent the calculated values of $dg/d\sigma$, given in the last column, derived from the components of $\underline{G}$ given in Table IV.

Plot	Stress direction	Magnetic-field direction	$dg/d\sigma$ (10^{-5} MPa^{-1})
a	[100]	[100]	20
b	[100]	[010]	8
c	[100]	[011]	22
d	[010]	[100]	15
e	[010]	[010]	4
f	[010]	[101]	2
g	[001]	[100]	−41
h	[001]	[010]	−17
i	[001]	[001]	−35
j	[110]	[001]	13
k	[001]	[110]	−28
l	[110]	[110]	10
m	[021]	[100]	−4
n	[201]	[010]	0
o	[201]	[102]	51
p	[021]	[012]	11

mined with stress applied parallel to the magnetic field. Finally, the lower three diagonal matrix elements were determined by combining data taken with stress perpendicular to the magnetic field with the results for the upper three diagonal elements. The values for the different elements of $\underline{G}$ are given in Table IV. The solid

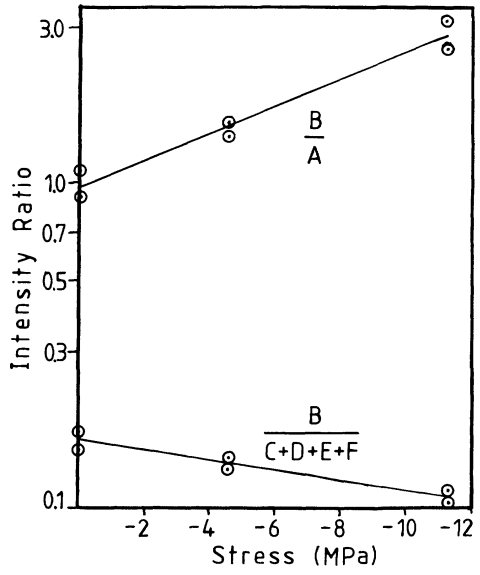

FIG. 8. Ratios of intensities for the differently oriented defects vs ⟨110⟩ uniaxial stress. The magnetic field is perpendicular to the stress. The labeling of the resonance lines follows that in the left-hand panel of Fig. 2. The data were taken at 4.2 K.

TABLE IV. The elements of the tensors $\underline{G}$ ($\underline{F}$) coupling the stress (strain) to the g values.

G (10^{-5} MPa^{-1})	F
$G_1=20$	$F_1=19$
$G_2=15$	$F_2=2$
$G_3=-41$	$F_3=-44$
$G_4=8$	$F_4=6$
$G_5=4$	$F_5=0$
$G_6=-17$	$F_6=-21$
$G_7=32$	$F_7=43$
$G_8=-7$	$F_8=-23$
$G_9=-35$	$F_9=-36$
$G_{10}=-40$	$F_{10}=-32$
$G_{11}=-77$	$F_{11}=-62$
$G_{12}=3$	$F_{12}=2$

curves in Fig. 7 are the predicted results using these values. The agreement with the experimental points is very good.[9]

It is often convenient to express the coupling to the strains $\underline{e}$ rather than the stresses $\underline{\sigma}$:

$$\delta\underline{g}=\underline{F}\cdot\underline{e}\ . \tag{5}$$

In Voigt notation this becomes

$$\begin{bmatrix}\delta g_{xx}\\ \delta g_{yy}\\ \delta g_{zz}\\ \delta g_{yz}\\ \delta g_{zx}\\ \delta g_{xy}\end{bmatrix}=\begin{bmatrix}F_1 & F_4 & F_7 & 0 & 0 & 0\\ F_2 & F_5 & F_8 & 0 & 0 & 0\\ F_3 & F_6 & F_9 & 0 & 0 & 0\\ 0 & 0 & 0 & F_{10} & 0 & 0\\ 0 & 0 & 0 & 0 & F_{11} & 0\\ 0 & 0 & 0 & 0 & 0 & F_{12}\end{bmatrix}\begin{bmatrix}e_{xx}\\ e_{yy}\\ e_{zz}\\ e_{yz}\\ e_{zx}\\ e_{xy}\end{bmatrix}\ . \tag{6}$$

Here, e_{ij} are, by convention, the Voigt or "engineering" strains, which are defined in terms of the tensor strains ϵ_{ij} as $e_{ii}=\epsilon_{ii}$, and $e_{ij}=\epsilon_{ij}+\epsilon_{ji}=2\epsilon_{ij}$ when $i\neq j$.

In the defect cubic axis system (x',y',z'), the strains and stresses are related by

$$\begin{bmatrix}e_{x'x'}\\ e_{y'y'}\\ e_{z'z'}\\ e_{y'z'}\\ e_{z'x'}\\ e_{x'y'}\end{bmatrix}=\begin{bmatrix}s_{11} & s_{12} & s_{12} & 0 & 0 & 0\\ s_{12} & s_{11} & s_{12} & 0 & 0 & 0\\ s_{12} & s_{12} & s_{11} & 0 & 0 & 0\\ 0 & 0 & 0 & s_{44} & 0 & 0\\ 0 & 0 & 0 & 0 & s_{44} & 0\\ 0 & 0 & 0 & 0 & 0 & s_{44}\end{bmatrix}\begin{bmatrix}\sigma_{x'x'}\\ \sigma_{y'y'}\\ \sigma_{z'z'}\\ \sigma_{y'z'}\\ \sigma_{z'x'}\\ \sigma_{x'y'}\end{bmatrix}\ . \tag{7}$$

For silicon, we use the values for the compliance constants $s_{11}=0.762\times10^{-5}$, $s_{12}=-0.213\times10^{-5}$, and $s_{44}=1.246\times10^{-5}$ MPa^{-1}.[10] Expressed in the defect principal axis system (x,y,z), this becomes

$$\begin{bmatrix}e_{xx}\\ e_{yy}\\ e_{zz}\\ e_{yz}\\ e_{zx}\\ e_{xy}\end{bmatrix}=\begin{bmatrix}s' & s'' & s_{12} & 0 & 0 & 0\\ s'' & s' & s_{12} & 0 & 0 & 0\\ s_{12} & s_{12} & s_{11} & 0 & 0 & 0\\ 0 & 0 & 0 & s_{44} & 0 & 0\\ 0 & 0 & 0 & 0 & s_{44} & 0\\ 0 & 0 & 0 & 0 & 0 & s'''\end{bmatrix}\begin{bmatrix}\sigma_{xx}\\ \sigma_{yy}\\ \sigma_{zz}\\ \sigma_{yz}\\ \sigma_{zx}\\ \sigma_{xy}\end{bmatrix}\ , \tag{8}$$

where $s'=(s_{11}+s_{12}+s_{44}/2)/2$, $s''=(s_{11}+s_{12}-s_{44}/2)/2$, and $s'''=2(s_{11}-s_{12})$. With Eq. (8), and its inverse, the elements of $\underline{F}$ were determined from those for $\underline{G}$. These are also given in Table IV.

2. *Defect alignment*

As shown in Figs. 6 and 8, the relative intensities of the resonance lines associated with the differently oriented defects change under uniaxial stress. (This was already noted by Woodbury and Ludwig in their earlier paper.[1]) We interpret this as a reorientation of the defect, the preferential alignment reflecting the energetically favored defect orientation under applied stress. The reorientation occurs faster than the response time of our measurements ($\sim$2–3 seconds), even at 2.2 K.

The shift in energy (ΔE) for an anisotropic defect in a cubic crystal under uniaxial stress has been given by Kaplyanskii.[11] Expressed in the defect cubic axis system, the result is

$$\Delta E=A_{x'x'}\sigma_{x'x'}+A_{y'y'}\sigma_{y'y'}+A_{z'z'}\sigma_{z'z'}+2A_{y'z'}\sigma_{y'z'}+2A_{z'x'}\sigma_{z'x'}+2A_{x'y'}\sigma_{x'y'}\ , \tag{9}$$

where A_{kl} are components of the symmetric piezospectroscopic tensor defined by Kaplyanskii to describe the coupling of the defect to external stress. For a defect of C_{2v} symmetry (rhombic I), Kaplyanskii has shown that $A_{x'x'}=A_{y'y'}$, and that $A_{y'z'}=A_{z'x'}=0$.[11]

Equation (9) can be written as a matrix product

$$\Delta E=\mathrm{Tr}(\underline{A}\cdot\underline{\sigma})=\mathrm{Tr}(\underline{B}\cdot\underline{\epsilon})\ , \tag{10}$$

where we have included the corresponding symmetric tensor $\underline{B}$, which is defined to describe the coupling to the strain tensor $\underline{\epsilon}$.

Assuming a Boltzmann distribution, we can write the ratio of the populations of two different defect orientations (n_i/n_j) in the presence of externally applied stress $\underline{\sigma}$ as

$$n_i/n_j=\exp[-(\Delta E_i-\Delta E_j)/k_BT]\ . \tag{11}$$

From the slope of an Arrhenius plot [$\ln(n_i/n_j)$ versus $|\sigma|$], we determine $(\Delta E_i-\Delta E_j)$ versus $|\sigma|$ for the differently oriented pairs of defects. (See Fig. 8.) With Eq. (9), this is sufficient to determine all of the components of $\underline{A}$ with the exception of the trace. (The breathing-mode distortion that shifts the energy of each of the six defect orientations by an equal amount reflects the trace of $\underline{A}$. Since this analysis compares relative energies and yields no information about absolute energy shifts, it determines only the traceless part of $\underline{A}$.) The

TABLE V. Principal values for the piezospectroscopic tensors $\underline{A}$ and $\underline{B}$. These values are extracted from the plots in Fig. 8.

Principal direction	A (10^{-5} eV/MPa)	B (eV/unit strain)
x	−0.34	+0.61
y	−3.68	−4.75
z	+4.02	+4.11

result of this analysis yields $A_{x'x'}=A_{y'y'}=-2.01\times10^{-5}$, $A_{z'z'}=4.01\times10^{-5}$, $A_{x'y'}=1.67\times10^{-5}$, eV/MPa.[12] A simple rotation of axes yields $\underline{A}$ in the defect principal axes system. This is given in Table V. The corresponding results for $\underline{B}$ are $B_{x'x'}=B_{y'y'}=-2.07$, $B_{z'z'}=4.11$, and $B_{x'y'}=2.68$ eV/unit strain. The values for $\underline{B}$ in the defect principal axis system are also given in Table V.

IV. DISCUSSION

As outlined in the Introduction, two different models have been suggested in the literature for the defect giving rise to the platinum EPR spectrum in silicon: (1) Woodbury and Ludwig[1] originally proposed on the basis of the apparent C_{2v} symmetry of the $\underline{g}$ and $\underline{A}$ tensors that the defect was an isolated substitutional Pt^- ion that had distorted off center in a ⟨100⟩ direction. (2) Henning and Egelmeers[3] subsequently proposed instead that an additional interstitial Pt^0 atom was nearby. Evidence cited for this was partially resolved structure on each of the lines in the EPR spectrum that could result from hyperfine interaction with the second Pt atom, and an apparent reduction to C_{1h} symmetry for the tensor $\underline{F}$ coupling the g values to lattice strain that they estimated in their strain-modulation detection technique.

The results that we have presented here strongly favor the original model of Woodbury and Ludwig—that of an off-center *isolated* substitutional Pt^- ion. The relevant results are the following: (1) By selective doping with ^{195}Pt and ^{198}Pt, we have demonstrated that there is no hyperfine evidence of a second Pt atom. The partially resolved shoulders on each EPR line apparently arise from hyperfine interactions with neighboring ^{29}Si neighbors. (2) The shifts in the g values that we measure versus applied uniaxial stress can be described satisfactorily by a strain coupling tensor $\underline{F}$ that has full C_{2v} symmetry, with no evidence of additional off-diagonal terms. (3) Reorientation of the defect is observed even at 2 K, revealing that the lowered C_{2v} symmetry results from an intrinsic distortion of a defect in an otherwise full T_d symmetry of the substitutional site.

Our result that the $\underline{F}$ tensor has C_{2v} symmetry conflicts with the conclusion of Henning and Egelmeers, who deduced large additional off-diagonal terms indicating C_{1h} symmetry. Let us therefore consider how these additional terms would have manifested themselves in our experiments, and whether we could have missed them. If the symmetry were C_{1h}, the number of orientationally degenerate defects would double compared to C_{2v}. That is, for each defect orientation in C_{2v} symmetry, there would be associated a pair in C_{1h} symmetry related to one another by a reflection through the yz plane. The additional off-diagonal elements of $\underline{F}$ indicating C_{1h} symmetry necessarily affect the pairs oppositely and should therefore produce splittings when stress is applied. No such splittings were observed in our experiments. For example, using the $\underline{F}$ tensor of Henning and Egelmeers, a splitting of ~100 G is predicted at $|\sigma|=10$ MPa for case "f" in Fig. 7 and Table III.[13] As the typical lines were only a few G wide, such a splitting would have been easily observed, but was not.

We are led to conclude therefore that for some reason the results of Henning and Egelmeers are in error and the true symmetry of the defect is C_{2v}. (We will not speculate on the possible source of the error except to point out that since these additional off-diagonal terms cans only produce symmetric splittings on the lines, their presence should not contribute in first order to the derivative-shaped lines detected in strain-modulation techniques anyway. This suggests an error in the analysis.)

It has been suggested earlier by one of us (G.D.W.) that the C_{2v} Pt^- distortion can be considered a Jahn-Teller distortion in analogy to that of the isolated negatively charged vacancy (V^-), which undergoes a similar distortion. In this "vacancy model," the defect is considered a neutral Pt atom with a d^{10} configuration in a negatively charged vacancy, the degeneracy arising from the partially filled t_2 vacancy orbitals in the gap. Our studies here of the defect alignment under stress reveal that the sense of the alignment is opposite to that for V^-. This is seen by noting that in the defect cubic axis system, the sign of each of the components of the $\underline{B}$ tensor for Pt^- is opposite to the corresponding one previously determined[14] for V^-. At first thought this would appear to be in conflict with the vacancy model. In the following paper (II), where the vacancy model is developed in detail, we will see, however, that this is not the case, the reversal resulting naturally in the model.

The observation of isotope effects on the g values by the two silicon neighbors that give rise to the resolved ^{29}Si hyperfine interactions is a most unusual result. In fact, to our knowledge, it is the first observation of such an effect for a defect in any semiconductor.[4] It is particularly surprising, therefore, that it arises from the neighboring atoms, rather than the core. In a sense it confirms the importance of the vacancy component of the center. It also suggests that there must be a strong vibronic character to this component of the defect in that the defect's overall magnetic properties apparently depend sensitively upon the amplitude of the zero-point vibrations of these neighbors. The defect is clearly statically distorted, as evidenced by the discrete spectrum for each orientation. However, it reorients easily at $T\sim2$ K, indicating an extremely lower barrier, and it manifests these remarkable vibronic effects as regards its neighbors. We are led to conclude, therefore, that, although the defect is statically distorted, it must be just barely so. It is tempting to conclude that it is the off-center motion of the heavy Pt ion that stabilizes the distortion, but that it remains strongly vibronic and free in its remaining aspects. In the follow-

ing paper (II), we will confirm certain aspects of this as revealed in the competition between the Jahn-Teller and spin-orbit effects.

V. CONCLUSION

A major purpose of this study was to resolve the question as to whether the EPR of platinum in silicon resulted from an isolated platinum ion or a platinum-platinum pair. We conclude that the original Woodbury and Ludwig model of an isolated substitutional Pt^- ion that spontaneously distorts off center in a $\langle 100 \rangle$ direction is correct. This conclusion is based upon the results of our experiments that show: (1) the partially resolved shoulders on each of the EPR lines are not the result of hyperfine interaction with a second Pt^0 atom, and (2) the symmetry of the center is C_{2v} as demonstrated both by the g tensor and its coupling to applied uniaxial stress.

Our experimental investigation has yielded other important and interesting results. We have fully resolved the superhyperfine interactions with the nearest pair of silicon atoms, and have found that the principal hyperfine axis on each is tilted by a rather large angle ($\sim 25°$) from the $\langle 111 \rangle$ direction normally expected for a dangling bond. Our stress alignment studies have shown that the defect can reorient at temperatures as low as ~ 2 K, consistent again with the isolated substitutional Pt^- model. From the signs of the components of the piezospectroscopic tensor, we conclude that the sense of the alignment for the Pt^- defect is opposite to that of the negatively charged vacancy. Finally, we have observed a shift in the g values depending upon the nuclear isotopes of the two nearest-neighbor silicon atoms.

The defect is statically distorted, each defect orientation with its own resolvable anisotropic spectrum of C_{2v} symmetry. However, the lack of a significant energy barrier for reorientation and the residual vibronic character evidenced by the isotope effects of the silicon neighbors suggests that it may be just barely so. We have suggested that the static stabilization may be the result of the fortuitous off-center motion of the heavy central Pt ion.

In the following paper (II), the vacancy model for the defect will be tested.

ACKNOWLEDGMENTS

The technical assistance of Dr. J. L. Newton in the operation of the 20-GHz spectrometer is gratefully acknowledged. One of us (R.F.M.) thanks Muhlenberg College for its partial support. This research was supported by the U.S. Navy Office of Naval Research under Contract Nos. N00014-76-C-1097, N00014-84-K-0025, and N00014-90-J-1264.

---

*Present address: Department of Physics, Muhlenberg College, Allentown, PA 18104.

[1]H. H. Woodbury and G. W. Ludwig, Phys. Rev. **126**, 466 (1962).

[2]G. W. Ludwig and H. H. Woodbury, in *Solid State Physics,* edited by F. Seitz and D. Turnbull (Academic, New York, 1962), Vol. 13, p. 223.

[3]J. C. M. Henning and E. C. J. Egelmeers, Phys. Rev. B **27**, 4002 (1983).

[4]Such an isotope effect has been reported for rare-earth defects in insulators by R. C. Newman, Adv. Phys. **18**, 545 (1969).

[5]F. G. Anderson, F. S. Ham, and G. D. Watkins, following paper, Phys. Rev. B **45**, 3287 (1992).

[6]G. D. Watkins, Physica B **117&118**, 9 (1983).

[7]One sample was allowed to cool slowly to room temperature while the diffusion oven cooled. This sample also showed the characteristic Pt^- spectrum, indicating that the quench is not essential.

[8]R. F. Milligan, F. G. Anderson, and G. D. Watkins, Phys. Rev. B **29**, 2819 (1984).

[9]The only significant departure is for the case "*d*" in Fig. 7. This line is particularly sensitive to off-axis $\langle 100 \rangle$ stress components and to stress alignment effects, making experimental determination difficult.

[10]J. J. Hall, Phys. Rev. **161**, 756 (1967).

[11]A. A. Kaplyanskii, Opt. Spektrosk. **16**, 602 (1964) [Opt. Spectrosc. (USSR) **16**, 329 (1964)].

[12]These experiments were also performed at a pumped-liquid-helium temperature of 2.2 K and yielded the same results.

[13]We note the error in Ref. 8 of Milligan, Anderson, and Watkins that should read 10^8 dyn/cm^2.

[14]G. D. Watkins, in *Deep Centers in Semicondcutors,* edited by S. T. Pantelides (Gordon and Breach, New York, 1986), p. 147.